A COMPARISON OF DUAL-TRACER TC-99M PERTECHNETATE AND TC-99M MIBI WITH AND WITHOUT SUBTRACTION SPECT IN THE DETECTION OF ABNORMAL PARATHYROID GLAND

Tawatchai Ekjeen[1,*], Chiraporn Tocharoenchai[1], Pawana Pusuwan[2], Eric C Frey[3]
[1]Department of Radiological Technology, Faculty of Medical Technology, Mahidol University, Bangkok, Thailand
[2]Division of Nuclear Medicine, Department of Radiology, Faculty of Medicine Siriraj Hospital, Bangkok, Thailand
[3]The Russell H Morgan Department of Radiology and Radiological Science, School of Medicine, Johns Hopkins University, Baltimore, MD, United States of America

ABSTRACT

The objective of this study was to compare dual-tracer Tc-99m pertechnetate (TcO4-) and Tc-99m MIBI (MIBI) with and without subtraction SPECT in the detection of abnormal parathyroid gland. Phantom population and an abnormal parathyroid with 100 mm^3 that was simulated at 6 clinical locations were simulated. Realistic projection data based on patient data were generated for TcO4- and MIBI using Monte Carlo simulation. The OS-EM with all compensations was used to reconstruct 3D images. The subtraction SPECT images were generated by subtracting MIBI SPECT from normalized TcO4- SPECT. Two techniques were evaluated including dual-tracer (MIBI+TcO4-) SPECT and subtraction SPECT. The CHO was used to evaluate image quality and AUC served as figure-of-merit. The AUC was 0.87 and 0.84 for dual-tracer SPECT and subtraction SPECT, respectively, and both methods were statistically different with p-value<0.05. The combination of Tc-99m pertechnetate SPECT and Tc-99m MIBI SPECT provided the best lesion detectability.

Keywords: Dual-tracer SPECT, Subtraction SPECT, Parathyroid gland, Simulation

1. INTRODUCTION

Several techniques for parathyroid imaging have been used involving different radiotracers and imaging protocols. The imaging technique that uses two different radiotracers refers to dual-tracer imaging. In dual-tracer imaging, Tc-99m MIBI is used in combination with Tc-99m pertechnetate or I-123, which is taken up only in thyroid gland. Simple visualization between 2 images can reveal different distribution of both radiotracers. In addition, the Tc-99m MIBI image can be digitally subtracted from normalized Tc-99m pertechnetate image to produce subtraction image.

Manuscript received on Oct 2, 2018; revised on Nov 29, 2018.
*Corresponding author E mail: tawatchai.ekj@mahidol.edu Department of Radiological Technology, Faculty of Medical Technology, Mahidol University, Thailand.

Parathyroid SPECT imaging is commonly used to confirm and identify abnormal parathyroid gland after performing conventional planar imaging. Moreover, SPECT imaging provides improved sensitivity in comparison to planar imaging and also increases reader confidence [1]. Several studies have been reported the use of dual-tracer subtraction SPECT for more precise localization of abnormal parathyroid gland and these studies were based on I-123 in combination with Tc-99m MIBI or Tc-99m tetrofosmin [2-5].

In Thailand, the most widely used radiotracer for imaging of thyroid gland is Tc-99m pertechnetate. In this study, we are interested in dual-tracer SPECT imaging using Tc-99m pertechnetate (TcO4-) and Tc-99m MIBI in the detection of abnormal parathyroid gland. Two techniques including dual-tracer SPECT without subtraction (MIBI+TcO4-) and with subtraction SPECT were evaluated and then compared.

2. MATERIALS AND METHODS

2.1. Phantom population

Populations of 9 male and 9 female phantoms based on the 3D eXtended CArdiac Torso (XCAT) phantom were generated. Three body sizes of phantoms for each gender including small (S), medium (M), and large (L) were modelled similar to clinical patient data with variations of neck size, chest size, and thyroid volume as shown in Table 1. Samples of 9 phantoms for each gender is shown in Figure 1. To simulate abnormal parathyroid gland, a spherical lesion with a volume of 100 mm^3 was generated and was placed at 6 clinically realistic locations in each phantom [6]. The lesion was simulated with a parathyroid to thyroid (P/T) uptake ratio of 1.0 [7]. This lesion size and uptake ratio were selected to model parathyroid hyperplasia that is commonly found in chronic renal failure patients and represent the limit of lesion detectability. A total of 108 phantoms with lesion and 18 phantoms without lesion were simulated in this study.

Table 1. Description of phantom population.

Organ size	Male			Female		
	S	M	L	S	M	L
Neck (cm)	35.7	40.3	44.9	35.7	40.3	44.9
Chest (cm)	74.9	83.6	92.3	73.3	78.3	83.4
Thyroid (cm^3)	10.7	15.7	20.7	10.7	15.7	20.7

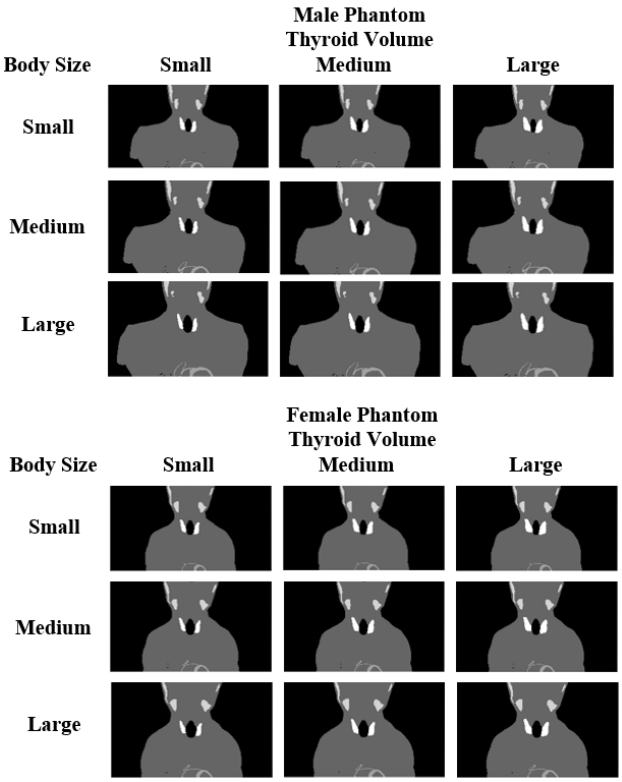

Figure 1. Phantom population of 9 male and 9 female anatomies.

2.2. Simulation of projection data for dual-tracer SPECT imaging

The SimSET/PHG Monte Carlo code combining with the angular response function (ARF) method was used to simulate projection data. A GE Infinia SPECT system with a 0.95 cm thick NaI(Tl) crystal was modelled. The system was equipped with low-energy high-resolution (LEHR) collimator and energy resolution was 9%. The data acquisition was simulated with 20% wide energy window centered at 140 keV, 120 views over 360° using a non-circular body-contouring orbit. For each phantom, projection data with low noise (4.6 billion of simulated photon) for Tc-99m of 4 organs including thyroid, parathyroid, salivary gland, and background were separately simulated with a pixel size of 0.1725 cm.

To generate projection data for dual-tracer SPECT imaging, the projection data with low noise of each organ were scaled based on clinical patient data obtained from TcO4- and MIBI with injected activity of 185 and 740 MBq, respectively, as shown in Table 2. After scaling, projection data of the 4 organs were then summed to generate the entire projection data. The projection data with lesion-present were simulated by adding the projection data of a spherical lesion to the entire projection data as shown in Figure 2.

In this study, projection data with multiple realizations of organ uptake for TcO4- and MIBI were generated. Thus a total of 2,160 projection data with lesion-absent for TcO4- and 1,080 projection data with lesion-present and 1,080 projection data with lesion-absent for MIBI were generated. For each projection data, Gaussian filter with a FWHM of 0.38 cm modelling an intrinsic spatial resolution was then applied. After that, the projection data were collapsed to a pixel size of 0.345 cm in a 128×128 projection image matrix, and finally, Poisson noise was added.

Table 2. Organ pixel value for Tc-99m pertechnetate and Tc-99m MIBI

Organ pixel value	Tc-99m pertechnetate		Tc-99m MIBI	
	Mean	Std. Dev.	Mean	Std. Dev.
Thyroid	349.0	271.7	674.5	365.2
Salivary	342.9	149.1	858.7	343.6
Background	16.6	5.2	55.0	16.6

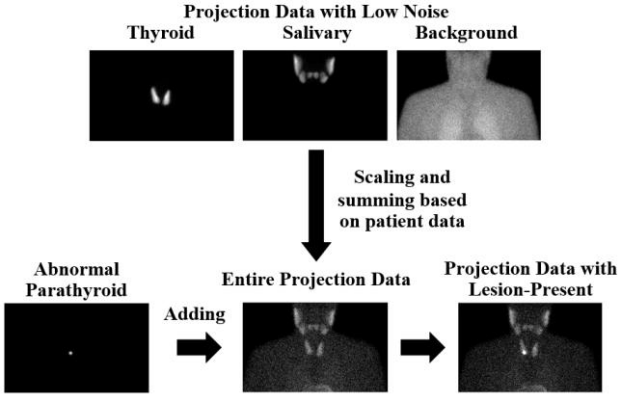

Figure 2. Generation of projection data with and without abnormal parathyroid gland.

2.3. Image reconstruction and post-reconstruction processing

2.3.1 Dual-tracer (MIBI+TcO4-) SPECT

All projection data of TcO4- and MIBI were reconstructed using OS-EM algorithm with compensation for attenuation (A), collimator-detector response (D), and scatter (S). Scatter compensation was implemented inside the reconstruction using the effective source scatter estimation (ESSE) method. In the reconstruction, 12 subsets with 10 projection data per subset were used and the number of iteration was varied from 1 to 20 iterations

including 1 to 10, 15, and 20 iterations. For each iteration, the Butterworth filter with order of 8 was applied with varying cut-off frequency from 0.20 to 0.34 cycle/pixel with increments of 0.02 cycle/pixel as shown in Figure 3. Each combination of iteration number and cut-off frequency of Butterworth filter was investigated to determine optimal parameters. The optimal parameter was investigated by using CHO and ROC analysis that was described below and the parameter giving the highest area under the ROC curve (AUC) was determined as the optimal parameter.

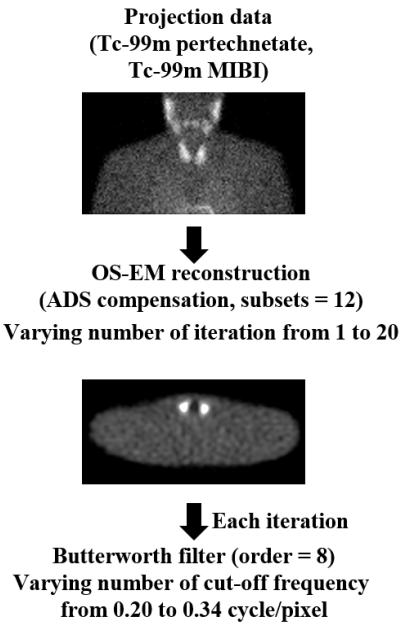

Figure 3. Image reconstruction and post-processing for dual-tracer SPECT.

2.3.2 Dual-tracer subtraction SPECT

The reconstructed images of TcO4- and MIBI obtained from each iterative update of the OS-EM reconstruction were used to produce subtraction SPECT. To generate subtraction images, firstly, the TcO4- SPECT images were normalized to obtain similar thyroid counts as MIBI SPECT images. The MIBI images were then subtracted from the normalized TcO4- images yielding the subtraction SPECT images. This subtraction process was performed for all iterative updates. After that, the subtraction images were then filtered using Butterworth filter with order of 8 and varying cut-off frequency from 0.20 to 0.34 cycle/pixel as shown in Figure 4. Similarly, optimal iteration number and cut-off frequency of Butterworth filter was investigated using CHO study.

2.3.3 Post-processing for channelized hoteling observer

All transaxial SPECT images were reformatted to generate 3D coronal and sagittal SPECT images. To generate the final images used in the CHO, an image slice centered at the lesion centroid was extracted into 32×32 matrix size and the same slice in the corresponding image without lesion. This process was performed for coronal and sagittal planes of SPECT images. Finally, the extracted images were windowed by mapping the maximum intensity to 255, truncating negative values to zero, and rounding the pixel value to an integer.

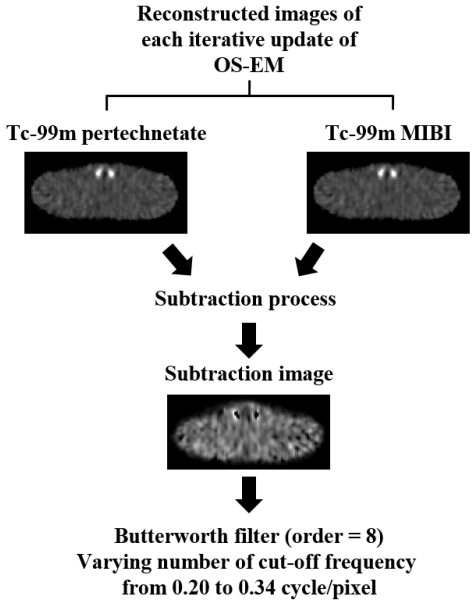

Figure 4. Subtraction process and post-processing for dual-tracer subtraction SPECT.

2.4. Channelized hoteling observer

A channelized hotelling observer (CHO) that predicts human observer performance was used to evaluate image quality. Anthropomorphic channels were used to incorporate the characteristic of human visual system into a model observer with a channel model comprised of 6 octave-wide non-overlapping rotationally symmetric annular frequency channels as shown in Figure 5. Each of the 6 channels was applied to 3 image planes including transaxial, coronal and sagittal images to generate an 18-element feature vector. For dual-tracer (MIBI+TcO4-) SPECT, 1,080 feature vectors with lesion-present and 1,080 feature vectors with lesion-absent were generated. Similarly, 1,080 feature vectors with lesion-present and 1,080 feature vectors with lesion-absent were generated for subtraction SPECT. A leave-one-out method was applied in the CHO study to generate the test statistics values. The test statistics were then analyzed using the LABROC4 program to compute the AUC. The AUC was used as the figure-of-merit and the highest AUC represents the highest lesion detectability.

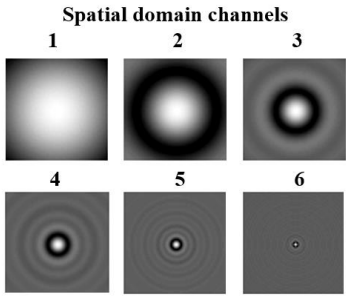

Figure 5. Spatial domain channels model characteristic of human visual system.

2.5. Data Analysis

In a comparison between dual-tracer (MIBI+TcO4-) SPECT and subtraction SPECT techniques, the AUC values obtained from both techniques with optimal number of update of OS-EM and cut-off frequency of Butterworth filter were tested for statistical significance of differences using the CLABROC program. The difference was statistically significant with p-value<0.05 at 95% confident interval.

3. RESULTS

The optimal number of update of OS-EM and cut-off frequency of Butterworth filter giving the highest AUC for dual-tracer (MIBI+TcO4-) SPECT and subtraction SPECT are shown in Table 3. According to the results, the optimal number of update of OS-EM algorithm using 12 subsets for both techniques was 36 and cut-off frequency of Butterworth filter with order of 8 for dual-tracer SPECT and subtraction SPECT was 0.28 and 0.22 cycle/pixel, respectively.

Table 3. Optimal number of update of OS-EM and cut-off frequency of Butterworth filter giving the highest AUC for both techniques.

Techniques	Optimal Parameters	
	#Update of OS-EM Reconstruction (#Subset = 12)	#Cut-off. Freq. ($pixel^{-1}$) of Butterworth Filter (Order = 8)
Dual-tracer SPECT	36	0.28
Subtraction SPECT	36	0.22

By using these optimal parameters, the highest AUC value for dual-tracer SPECT and subtraction SPECT was 0.87 and 0.84, respectively. In addition, dual-tracer SPECT was compared with subtraction SPECT using paired t-test as shown in Table 4. This result showed that dual-tracer SPECT was statistically significant different from subtraction SPECT with p-value < 0.05 at 95% confident interval.

Table 4. A comparison of AUC values between dual-tracer SPECT and subtraction SPECT with optimal parameters.

Method1	Method2	AUC1	AUC2	P-value
Dual-tracer SPECT	Subtraction SPECT	0.87	0.84	0.00

Sample of coronal SPECT images of dual-tracer SPECT and subtraction SPECT are shown in Figure 6. In dual-tracer SPECT, TcO4- image was visualized together with MIBI image. Comparing with TcO4- image, the abnormal parathyroid gland was clearly seen at inferior pole of right thyroid lobe as indicated by white arrow. In subtraction SPECT, the MIBI images were subtracted from TcO4- images removing thyroid gland out of the images. As a result, the subtraction images obviously revealed the abnormal parathyroid gland. However, the subtraction images look noisier than TcO4- and MIBI images. In addition, lumpy noise textures (noise blobs) distributed over subtraction images are prominent and obviously seen.

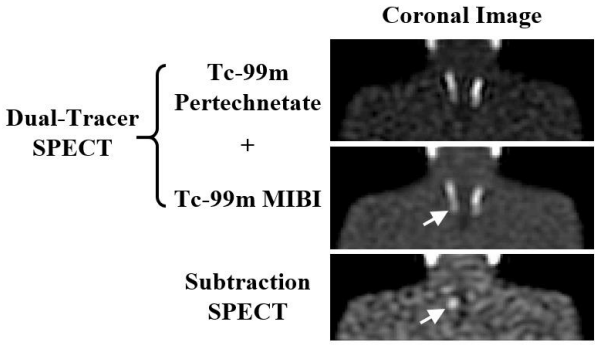

Figure 6. Sample of coronal SPECT images of dual-tracer (MIBI+TcO4-) SPECT and subtraction SPECT. The abnormal parathyroid gland was positioned at inferior pole of right thyroid lobe as indicated by white arrow.

4. DISCUSSION

Parathyroid imaging has been a widely used method for localizing hyperfunctioning parathyroid glands. Oversecretion of parathyroid hormone (PTH) from these abnormal glands results in hyperparathyroidism which plays an important role in the adverse effects to many organs [8]. For parathyroid imaging, SPECT offer several advantages over planar imaging including 3-dimensional (3D) images, greater contrast, better lesion size estimation and lesion localization [5].

In this study, we explored dual-tracer Tc-99m pertechnetate and Tc-99m MIBI with and without subtraction SPECT in the detection of abnormal parathyroid gland. The results of this study showed that both techniques provided good performance (AUC values >0.80) in the detection of abnormal parathyroid gland. Similarly, several studies reported that dual-tracer subtraction SPECT provided high sensitivity ranged from 80% - 100% in the detection and localization of abnormal

parathyroid glands [2-4, 9]. In addition, dual-tracer SPECT gave significantly better detectability than using subtraction SPECT alone.

It has been reported in several studies that Tc-99m MIBI parathyroid SPECT improved the detection of abnormal parathyroid gland [1, 10-11]. In addition, previous study showed that MIBI parathyroid SPECT with optimized reconstruction parameters and all compensations provided the highest improvement of image quality and lesion detectability [12]. For these reasons, when combining MIBI SPECT with additional information of TcO4- SPECT, the abnormal parathyroid gland can easily be detected.

For subtraction SPECT, the background noise level was increased due to subtraction technique. In addition, the compensation for collimator-detector response during reconstruction restores mid-range of spatial frequencies and gives rise to a correlated noise texture (noise blobs) distributed over SPECT images [12-13]. As a result, these noise textures exhibited more prominent and can be obviously seen in the subtraction images. It is known that the noise correlations have an adverse effect on the ability of the observer to detect lesion in background [14]. Thus these noise blobs similar to parathyroid lesion lead to false-positive result and the detection performance can be reduced.

In parathyroid imaging, the most common cause of false-positive results is the presence of thyroid nodule [1, 15]. Additional information of thyroid images using TcO4- may be useful for identifying thyroid disease. By using dual-tracer subtraction SPECT, patient's position and motion should be aware during separately data acquisition of each radiotracer. Suboptimal registration between two images of TcO4- and MIBI due to separate acquisition may lead to incorrect subtraction and misinterpretation.

5. CONCLUSION

The combination of Tc-99m pertechnetate SPECT and Tc-99m MIBI or dual-tracer (MIBI+TcO4-) SPECT provided better detection performance than dual-tracer subtraction SPECT. In subtraction SPECT images, the increasing background noise level due to subtraction technique may affect detection performance. In clinical application, additional information of TcO4- thyroid SPECT in combination with MIBI parathyroid SPECT might be a good option for localizing abnormal parathyroid gland.

6. ACKNOWLEDGEMENT

The authors would like to thank Division of Medical Imaging physics, Department of Radiology, Johns Hopkins University for providing and supporting XCAT phantom, simulation code, and CHO used in this study.

REFERENCES

[1] D. Taieb, E. Hindie, G. Grassetto, P.M. Colletti, D. Rubello, "Parathyroid scintigraphy, when, how, and why? A concise systematic review," Clin. Nucl. Med., vol. 37, pp. 568-574, 2012.

[2] M. Sommerauer, C. Graf, N. Schafer, G. Huber, P. Schneider, R. Wuthrich, C. Schmid, H. Steinert, "Sensitivity and specificity of dual-isotope ^{99m}Tc-Tetrofosmin and ^{123}I sodium iodide single photon emission computed tomography (SPECT) in hyperparathyroidism," PLoS One, vol. 10(6), pp. 1-11, 2015

[3] D.R. Neumann, C.B. Esselstyn, A.M. Madera, "Sestamibi/iodine subtraction single photon emission computed tomography in reoperative secondary hyperparathyroidism," Surgery, vol. 128, pp. 22-28, 2000.

[4] D.R. Neumann, C.B. Esselstyn, R.T. Go, C.O. Wong, T.W. Rice, N.A. Obuchowski, "Comparison of double-phase Tc-99m sestamibi with I-123-Tc-99m sestamibi subtraction SPECT in hyperpara-thyroidism," AJR, vol. 169, pp. 1671-1674, 1997.

[5] D.R. Neumann, C.B. Esselstyn, A. Madera, C.O. Wong, M. Lieber, "Parathyroid detection in secondary hyperparathyroidism with I-123/Tc-99m sestamibi subtraction single photon emission computed tomography," J. Clin. Endocrinol. Metab., vol. 83, pp. 3867-3871, 1998.

[6] H.K. Eslamy, H.A. Ziessman, "Parathyroid scintigraphy in patients with primary hyperparathyroidism: ^{99m}Tc sestamibi SPECT and SPECT/CT," Radiographics, vol. 28, pp.1461-1476.

[7] M.J. O'Doherty, A.G. Kettle, P. Wells, R.E.C Collins, A.J. Coakley, "Parathyroid imaging with Technetium-99m-sestamibi: preoperative localization and tissue uptake studies," J. Nucl. Med., vol. 33, pp. 313-318, 1992.

[8] P. Woraratsoontorn, C. Bunluechokchai, W. Rattanawong, W. Ussawawongaraya, "Wavelet and fourier transform analysis of ECG signals in peritoneal dialysis patients with hyperparathyroidism," IJABME., vol.8, pp. 17-21, 2015.

[9] A.M. Woods, A.A. Bolster, S. Han, F.W. Poon, D. Colville, Shand J, J.B. Neilly, "Dual-isotope subtraction SPECT-CT in parathyroid localization," Nucl. Med. Commun., vol. 38, pp. 1047-1054, 2017.

[10] M.O. Oksuz, H. Dittmann, C. Wicke, K. Mussig, R. Bares, C. Pfannenberg, S.M. Eschmann, "Accuracy of parathyroid imaging: a comparison of planar scintigraphy, SPECT, SPECT-CT, and C-11 methionine PET for the detection of parathyroid adenomas and glandular hyperplasia," Diagn. Interv. Radiol., vol. 17, pp. 297-307, 2011.

[11] M. Lorberboym, T. Ezri, P.P. Schachter, "Preopertative technetium Tc-99m sestamibi SPECT imaging in the management of primary hyperparathyroidism in patients with concomitant multinodular goiter," Arch. Surg., vol. 140, pp. 656-660, 2005.

[12] T. Ekjeen, C. Tocharoenchai, P. Pusuwan, G.S.K. Fung, M. Ghaly, Y. Du, E.C. Frey, "Optimization and evaluation of reconstruction-based compensation methods and reconstruction parameters for Tc-99m MIBI parathyroid SPECT," Phys. Med., vol. 31, pp. 159-166, 2015.

[13] H. Mahani, G. Raisali, A. Kamali-Asl, M.R. Ay, “Collimator-detector response compensation in molecular SPECT reconstruction using STIR framework,” Iran. J. Nucl. Med., vol. 25, pp. 26-34, 2017.

[14] D.J. de Vries, M.A. King, E.J. Soares, B.M. Tsui, C.E. Metz, “Effects of scatter subtraction on detection and quantification in hepatic SPECT,” J. Nucl. Med., vol. 40, pp. 1011-1023, 1999.

[15] J.R. Smith, M.E. Oates, “Radionuclide imaging of the parathyroid glands: patterns, pearls, and pitfalls,” RadioGraphics, vol. 24, pp. 1101-1115, 2004.